Scientific African 3 (2019) e00075

Contents lists available at ScienceDirect

Scientific African

journal homepage: www.elsevier.com/locate/sciaf

Adsorptive Fe-nanoparticles mediated by *Musa sapientum* peels extract as anticorrosion additive for aqueous oilfield descaling solution

Ekemini Ituen[a,b,*], Victor Mkpenie[a], Ekere Ekemini[b]

[a] *Materials and Oilfield Chemistry Research Group, Department of Chemistry, Faculty of Science, University of Uyo, Uyo, Nigeria*
[b] *Materials Research Laboratory, Center for Sustainable Education and Training, C-SET, Uyo, Nigeria*

ARTICLE INFO

Article history:
Received 4 January 2019
Revised 10 April 2019
Accepted 24 April 2019

Keywords:
Banana peels extract
Agro-waste
Bananadine
Adsorption
Acid wash

ABSTRACT

Banana (*Musa sapientum*) peel is a biodegradable and non-toxic agricultural waste that can be readily and sustainably obtained. Its ethanolic extract was used to mediate the synthesis of nanoparticles using iron (ii) chloride ($FeCl_2$) and investigated as anticorrosive additive for mild steel in laboratory simulated descaling solution. The essence was check if improved efficiency could be obtained by reducing the crude extract to nanoparticles. Thermogravmetric and electrocanalytical techniques were used to determine the inhibition efficiency. Results reveal that 10 mL *Musa sapientum* extract-iron oxide nanoparticle (Fe-MSE Nano) was 94.4% efficient compared to the crude extract which was 72.1% efficient in 1.0 M HCl corroding solution at 30 °C. Charge transfer resistance from impedance measurements increases as concentration of nanoparticle per volume of descaling solution increases owing to adsorption of molecules of the composites. Fe-MSE Nano acts as mixed type inhibitor, predominantly inhibiting anodic oxidation reaction. The steel surface was found to be morphologically smoother than without the Fe-MSE Nano as observed by scanning electron microscopy (SEM). Adsorption behavior of the major compound in the peels extract, bananadine, was modeled theoretically on Fe(1 1 1) surface using density functional theory. Theoretical parameters such as frontier molecular orbitals energies, rigid adsorption energy, and deformation energy were calculated. Fukui analysis and Forcite neutron scattering analysis were also performed and nitrogen site (N8) is predicted as the active adsorption site. Based on results obtained, Fe-MSE Nano would make a more efficient anticorrosive additive for steel in oilfield descaling solution than the crude extract.

© 2019 The Authors. Published by Elsevier B.V. on behalf of African Institute of Mathematical Sciences / Next Einstein Initiative.
This is an open access article under the CC BY license.
(http://creativecommons.org/licenses/by/4.0/)

Introduction

Scaling is a major problem in the petroleum industry and is associated with some operations such as stimulation, production and transportation. Scales generate when the solution becomes supersaturated maybe due to temperature changes during injection operations [1]. Scales can also be formed when two solutions that are capable of precipitating are brought

* Corresponding author at: Department of Chemistry, Faculty of Science, University of Uyo, Uyo, Nigeria.
E-mail address: ekeminiituen@uniuyo.edu.ng (E. Ituen).

https://doi.org/10.1016/j.sciaf.2019.e00075
2468-2276/© 2019 The Authors. Published by Elsevier B.V. on behalf of African Institute of Mathematical Sciences / Next Einstein Initiative. This is an open access article under the CC BY license. (http://creativecommons.org/licenses/by/4.0/)

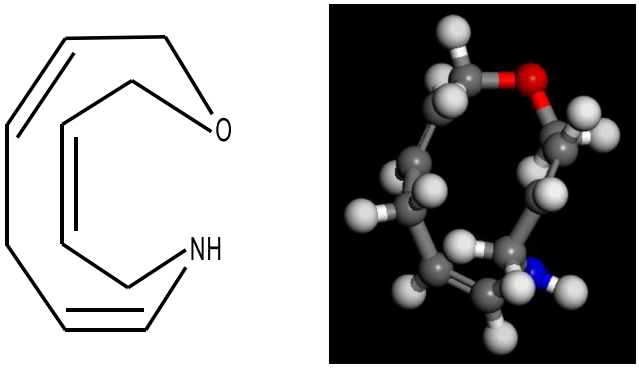

(a) (b): Blue = N; Red = O; Gray = C; White = H

Fig. 1. (a). Molecular structures of bananadine (b) Structure optimized at DFT/GGA-PW91.

together. For instance, the contact of calcium ions from dissolved fines with hydrogen fluoride from reservoir stimulation fluid is likely to precipitate calcium fluoride scales [2].

$$Ca^{2+}_{(aq)} + 2HF_{(aq)} \rightarrow CaF_{2(s)} + 2H^{+}_{(aq)} \tag{1}$$

Sometimes, one or more types of inorganic deposit alongside with other organic debris, sand, precipitates and corrosion products constitute scales. Common scales encountered in the field include calcium carbonate, iron carbonate, barium sulphate, iron sulphides, gypsum, strontium sulphate and magnesium salts. Details on scales and its chemistry is available in literature [3,4]. Scale formation is a setback as it affects flow and continuous production from existing reserves that produce brine [5]. Scaling and corrosion mostly occur simultaneously [6]. In fact, many wells have been abandoned prematurely because scaling and corrosion are poorly managed [7].

One of the ways scales are removed is by acid washing especially in oil and gas production. Research has shown that the most effective solution for descaling by acid wash is 5% HCl [8]. This concentration is higher than 1.0 M, therefore corrosion problems usually generate. Corrosion inhibitors are usually added to the descaling solution to protect the steel surface from corrosive attack due to the acid [9]. The function of the corrosion inhibitor is to retard the rate of corrosion of the steel. Otherwise, corrosion of steel structural materials could result in failure of materials, spills and perhaps disasters which would be expensive to manage.

Some chemical corrosion inhibitors used in the field are limited by toxicity and high cost. Toxic corrosion inhibitors can cause environmental pollution especially those that are non-biodegradable. This is why research into environmentally benign corrosion inhibitors from cheap sources is very active, hence the reason an agricultural waste is being investigated in this study. Many plant extracts have been used as corrosion inhibitors, many of which show good inhibitive potentials [10–12]. However, their inhibitive effects decline at high temperatures. It is believed that materials react faster at the nano scale. This study stems from the belief that and modifying plant extracts chemically into nanoparticles could improve their thermal stabilities, enhance their adsorptive tendencies, and improve their corrosion inhibition efficiencies.

Previously, *Musa sapientum* peels extract (MSE) has been reported to be an effective corrosion inhibitor for carbon steel in sea water [13]. Nanoparticles have also been prepared from MSE [14,15] and reported to exhibit antimicrobial [16] and antibacterial [17] activities against the associated agents. Though there are scanty reports on the use of plant-based nanoparticles as other oilfield chemicals such as mud additives [18,19], surfactants [20,21] and corrosion inhibitors [22–24]. After thorough literature search and to the best of our knowledge, there is no report on the use of MSE nanoparticle as corrosion inhibitor. In other to fill this gap, we investigated Fe-MSE nanoparticles to compare the efficiency with that of the crude extract under similar conditions. Phytochemical profile of MSE peels reveals that it is highly rich in bananadine ((3Z,7Z,10Z)−1-oxa-6-azacyclododeca-3,7,10-triene) which contains heteroatoms, double bond and pie-electron systems [13] as shown in Fig. 1. Since these sites present in the phytocompounds in MSE, the choice of Fe-MSE nano is motivated by the consideration that they could act as adsorption sites as reported for some established corrosion inhibitors [25]. Fe is also selected as the metal ion since it has vacant d-orbitals for electron exchange and can easily interact with similar Fe ions on the steel surface.

In this study, the oilfield descaling liquor is simulated with aqueous 1 M HCl solution. Weight loss technique is used to estimate the rate of corrosion of the simulated descaling liquor. The tests are conducted at different temperatures to mimic geothermal gradients in fields. Further insight into the interaction, between the iron surface and the active compound in MSE is explored at the level of density functional theory (DFT) which is a potent tool for modeling interactions between molecules (adsorbates) and surfaces. Although many of such theoretical studies exist on densely packed Fe (0 0 1) and Fe(1 1 0) surfaces [26, 27], as well as the open Fe(1 1 1) surface [28] using other adsorbates, information on bananadine-Fe(1 1 1) interaction is also clearly lacking. The choice of Fe(1 1 1) surface for this studies stems from the believe that Fe(1 1 1) has high catalytic activity because of its structure [29]. The study of bananadine adsorption on the Fe (111) surface at low

coverage at the level of DFT will provide a detailed picture of the geometric, energetic and electronic structure of the clean and adsorbed surface, as well as adsorption mechanism on the Fe(111) surface for the first time.

Materials and methods

Metal specimens

The mild steel sheets used were purchased from Construction Materials market, Oron Road, Uyo Nigeria. It was mechanically press-cut into coupons of dimension 4.0 cm × 4.0 cm and a small hole made near the upper edge for the insertion of glass hook. The coupons were abraded with silicon carbide paper of grade 1000, degreased with ethanol, dried in acetone and then stored in a moisture free desiccator before use in corrosion studies.

Preparation of Musa sapientum *peel extract*

Banana peels were obtained as wastes from a local restaurant in Uyo, Akwa Ibom State, Nigeria and transported to the Chemistry laboratory on the same day. The peels were washed with deionized water and air-dried in the laboratory. The dried substrates were then blended into fine powder and soaked in analytical grade ethanol for 48 h. The resulting mixture was filtered using Whatman No.1 filter paper and the filtrate obtained was concentrated using rotary evaporator at low vacuum pressure [26]. The extracts obtained were stored in sealed vials until used for the analysis.

Preparation of nanoparticles-extract composite (Fe-MSE nano)

10 g of extract was dissolved in 1000 mL of distilled water to obtain stock solution of extract of concentration of 10 g/L. $FeCl_2$ of concentration 1×10^{-3} M was used for the preparation of nanoparticle-extract composite according to a method reported elsewhere [27]. Different amounts (1 mL, 2 mL, 5 mL and 10 mL) of the extract were added to 40 mL of the metal ion separately, stirred gently for 1 h at room temperature and observed keenly until there was a color change, signifying the end of the reaction and formation of nanoparticle [30].

Thermo-gravimetric analyses

Previously weighed mild steel coupons were each suspended by a glass hook and completely immersed into 1.0 M HCl solution in separate beakers maintained at 30 °C in a thermostatic water bath. The coupons were retrieved from their corroding solution after five (5) hours, washed with 1.0 M NaOH containing 4.0 g of Zinc dust, rinsed in acetone, dried in air and reweighed [25]. The difference in weights was recorded as weight loss. This was repeated at temperatures 40 °C, 50 °C and 60 °C for both the crude MSE and the composites. The inhibition efficiency (%*I*), corrosion rate (*CR,* mmpy) and degree of surface coverage (θ) were computed using Eqs. (2)–(4), respectively [31].

$$CR = \frac{(m_o - m_1)}{At} \tag{2}$$

$$\%I = 100\left(\frac{CR_a - CR_i}{CR_a}\right) \tag{3}$$

$$\theta = 0.01\ I \tag{4}$$

where m_o and m_1 are the weights of the coupons before and after immersion in the test solutions, A is the cross sectional area of the coupons, t is the immersion time, CR_a and CR_i are the corrosion rates of steel in the acid and inhibited solutions.

Electrochemical monitoring techniques

Electrochemical measurements were conducted using electrochemical workstation consisting of the conventional three electrode set up (saturated calomel electrode (SCE) as reference electrode, platinium as counter electrode and steel coupon as working electrode). Open circuit scan was run for 30 min to achieve steady open circuit potential (OCP). Electrochemical impedance measurements (EIS) were conducted at frequency of 10^5–10^{-2} Hz at 30 °C. Voltage of −0.15 V to + 0.15 V *vs.* OCP at 0.2 mV/s scan rate was set for potentiodynamic polarization (PDP) measurements. Experiments were conducted using the uninhibited and inhibited acid solution. Charge transfer resistance and corrosion current densities were used to calculate the inhibition efficiencies for EIS (ε_{EIS}) and PDP (ε_{PDP}) measurements according to Eqs. (5) and (6) respectively.

$$\varepsilon_{EIS} = 100\left(\frac{R_{ctI} - R_{ctB}}{R_{ctI}}\right) \tag{5}$$

$$\varepsilon_{PDP} = 100\left(1 - \frac{I^i_{corr}}{I^b_{corr}}\right) \tag{6}$$

where R_{ctB} and R_{ctI} are measured charge transfer resistances without and with inhibitor, respectively and I^b_{corr} and I^i_{corr} are the measured corrosion current densities without and with inhibitor respectively. The magnitude of the double layer capacitance

(C_{dl}) of the adsorbed film was calculated from constant phase element (CPE), constant (Y_o) and charge transfer resistance (R_{ct}) using Eq. (7).

$$C_{dl} = \left(Y_0 R_{ct}^{n-1}\right)^{\frac{1}{2}} \tag{7}$$

where n is a constant obtained from the phase angle given that ($j^2 = -1$), α is the phase angle of the CPE and $n = 2\alpha/(\pi)$.

Scanning electron microscopy

Mild steel coupons of size 1 cm × 2 cm were abraded to mirror finish. The SEM images were recorded before and after immersion in 1 M HCl for 5 h. This was repeated with a coupon immersed in HCl containing the highest concentration of Fe-MSE Nano. The images obtained without and with Fe-MSE Nano were compared.

Computational methods

Computational results were obtained by BIOVIA Materials Studio version 17.1 (2017) software programs from Dassault Systèmes BIOVIA (United States). Initial geometry optimization of bananadine was performed with the DMol^3 program [32] at DFT level of theory using general gradient approximation (GGA) with Perdew and Wang (PW91) exchange-correlation functional [33]. A dispersion correction for DFT (DFT-D) using semi-empirical dispersion-correction approach of Ortmann, Bechstedt and Scheffler [34] was employed to correct non-bonding interactions. The double numeric basis set with polarization function (DNP) was used. The tolerance of energy, gradient and displacement convergence were set to 1×10^{-5} Ha, 2×10^{-3} Ha/Å and 5×10^{-3} Å, respectively. A Fermi smearing of 0.005 Ha was used to improve computational performance. The optimization was performed under spin unrestricted condition with no symmetry. The optimized structure of bananadine is shown in Fig. 1.

Fe(111) surface was cleaved from Fe crystal (body centered 3D cubic) with lattice parameters $a = b = c = 2.8664$ and $\alpha = \beta = \gamma =$ 90 °C. The fractional thickness of the cleave plane was set to 6.0, indicating 6 layers of Fe atoms. The 6 layers were chosen to give a sufficient depth so that the bananadine molecule will only be involved in non-bond interactions with Fe atoms in the layers of the surface. A 3 × 3 supercell was created from the cleaved surface and a vacuum slab was built with thickness varying from 15–30 Å in order to determine the minimum vacuum thickness that will ensure sorbate-only interaction with the surface atoms without interaction with periodic image of the bottom layer of atoms in the surface. The vacuum thickness was then fixed at 30 Å which was sufficient to prevent any non-bond interactions between the next repeat unit and either the Fe surface or the bananadine molecule. The periodic cell used for the simulation were characterized by lattice parameters: $a = b = 12.16$ Å, $c = 39.10$ Å, $\alpha = \beta =$90 °C and $\gamma =$ 120 °C. The adsorption of bananadine on Fe(1 1 1) surface was modeled using the Adsorption Locator of Materials Studio BIOVIA. Adsorption Locator simulates a substrate loaded with an adsorbate or an adsorbate mixture of a fixed composition and a low energy adsorption site is identified by carrying out a Monte Carlo search of the configurational space of the substrate-adsorbate system as the temperature is slowly decreased. Adsorption Locator uses forcite engine for its calculation. The optimized structure (from Dmol^3) was re-optimized using forcite with Smart algorithm. The converge criterion judged by the energy, force and displacement, respectively were 1×10^{-4} kcal/mol, 5×10^{-3} kcal/mol/ Å and 5×10^{-5} Å. The forcefields, COMPASS (Condensed-phase Optimized Molecular Potentials for Atomistic Simulation Studies), pcff (polymer consistent forcefield) and cvff (consistent-valence forcefield) were tested to determine the optimized structure with the lowest energy. COMPASS forcefield which recorded the lowest energy of −27.194 kcal/mol compared to pcff (−15.050 kcal/mol) and cvff (35.482 kcal/mol) forefields was chosen to model the adsorbate-Fe(1 1 1) interaction. The Adsorption Locator calculation was performed by simulated annealing using the COMPASS forcefield. The simulated annealing procedure uses a single reference structure and monotonically decreases the simulation temperature. The annealing procedure starts from a temperature high enough to allow the system explore to the entire conformational space. The first three layers of Fe atoms were used independently as target atoms for the adsorbate—surface interaction (Fig. 7(a)), starting from the top layer, Fe_{top} (surface atoms), through the second layer, Fe_{shal} (shallow atoms) to the third layer, Fe_{deep} (deep atoms), respectively and investigating the energy distribution and low energy configuration. The maximum adsorption distance was varied between 5 and 30 Å to investigate the minimum distance that would give all possible configurations of interaction between one molecule of babanadine loaded, and the Fe surface atoms.

Results and discussion

Formation of Fe-MSE nanoparticles

MSE mediated the formation of the iron nanoparticles within a duration of 20 min resulting in a change of the shade of the MSE to a brownish colloidal solution. Many literature reports reveal that when plant extract mediated nanoparticles are formed and completely developed, the color of the solution would be yellowish through brown to dark brown [30,35]. This is so because different macromolecules from the extracts catalyze and stabilize the formation of the nanoparticles [30]. The bananadine present in MSE could have played catalytic and stabilization roles. Spectroscopic and microscopic analyses of the nanoparticles could reveal the active ingredients involved in the biogenetic synthesis. In addition, the nanoparticles obtained were stable, and did not deteriorate or aggregate. These results are similar with literature reports [30].

Table 1
Weight losses (g) of mild steel in 1 M HCl without and with crude MSE and Fe-MSE Nano solutions at 30 – 60 °C.

Test solution	30 °C	40 °C	50 °C	60 °C
1 M HCl	0.7838	1.5525	2.5347	3.8729
MSE	0.2184	0.4864	0.9424	1.7272
1 ml Fe-MSE Nano	0.1184	0.3040	0.5552	0.9872
2 ml Fe-MSE Nano	0.0912	0.2304	0.4008	0.7401
5 ml Fe-MSE Nano	0.0688	0.1584	0.3368	0.6200
10 ml Fe-MSE Nano	0.0416	0.1040	0.2688	0.4960

Initial weights of coupons = (7.2 ± 0.3) g.

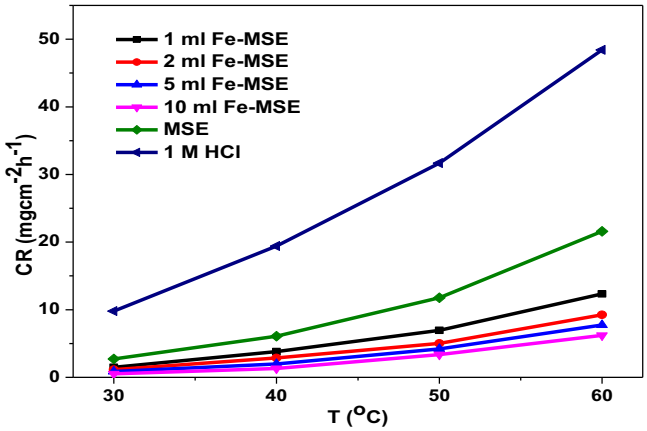

Fig. 2. Variation of corrosion rate with temperature for the corrosion of mild steel in 1 M HCl containing MSE and Fe-MSE nanoparticles.

Table 2
Corrosion rates (mmpy) of mild steel in 1 M HCl without and with crude MSE and Fe-MSE nano solutions at 30–60 °C.

Test solutions	30 °C		40 °C		50 °C		60 °C	
	CR	*% I*	*CR*	*% I*	*CR*	*% I*	*CR*	*% I*
1 M HCl	9.80	–	19.41	–	31.68	–	48.41	–
MSE	2.73	72.1	6.08	68.7	11.78	62.8	21.59	55.4
1 ml Fe-MSE	1.48	84.9	3.80	80.4	6.94	78.1	12.34	74.5
2 ml Fe-MSE	1.14	88.4	2.88	87.7	5.01	84.2	9.25	80.9
5 ml Fe-MSE	0.86	91.2	1.98	89.8	4.21	86.7	7.75	84.0
10 ml Fe-MSE	0.52	94.7	1.30	93.3	3.36	89.4	6.20	87.2

Weight loss, corrosion rate and inhibition efficiency

Weight loss values obtained with 1 M HCl is higher than that of the extracts, but lowest weight losses were obtained with the nanoparticles (see Table 1). Corrosion rate follows a similar trend as weight loss, and increases as temperature increases (Fig. 2). However, inhibition efficiency of the nanoparticles is higher than that of the crude extract measured in this study (Table 2). Previous reports on efficiency of MSE extracts in 1 M HCl show that it was 66.8% and 65.9% efficient as measured by gasometric and thermometric techniques respectively [31]. In another report, 0.03 wt.% and 0.07 wt.% of banana peels extract was found to be 68.9% and 79.4% efficient in 1 M HCl at room temperature [32]. The results obtained in these studies are comparable with that of the present study for the crude extract. However, when prepared into nanoparticles, the efficiency increased even at very small extract concentration. This demonstrates that the biomaterial is more effective at nanoscale than in the crude form. This could be due to coordination and complexation reaction between the bananadine molecules by the metal ion used in the synthesis of the Fe-MSE. Such a reaction can result in a complex with high molecular weight, increased melting/degradation temperature, hence improved inhibition efficiency.

Electrochemical measurements

Mild steel is an alloy of many metals; hence various oxidation reactions could occur at the anode. Typically, the anodic oxidation reaction may be represented by Eq. (8). For iron, which is the main element in mild steel, the oxidation reaction

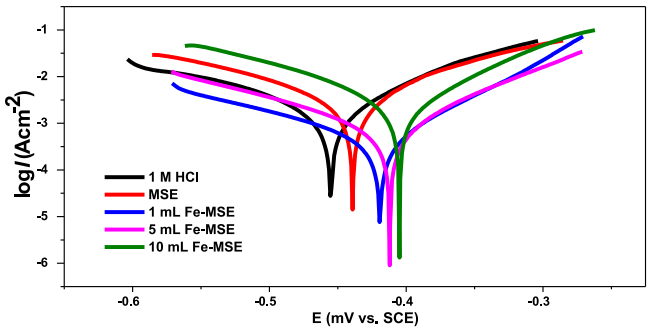

Fig. 3. Tafel plots for mild steel corrosion inhibition in simulated descaling solution without and with MSE and different concentrations of Fe-MSE Nano.

Table 3
PDP parameters for mild steel corrosion in 1 M HCl without and with different concentrations of MSE and Fe-MSE Nano.

Parameters	1 M HCl	MSE	1 mL Fe-MSE	5 mL Fe-MSE	10 mL Fe-MSE
β_a (mV/decade)	112.2	96.6	91.8	99.4	97.2
β_c (mV/decade)	77.6	74.9	79.2	81.1	88.6
I_{corr} (μA)	811.6	228.8	116.9	60.9	30.8
E_{corr} (V)	−0.455	−0.438	−0.418	−0.411	−0.404
ε_{PDP} (%)	–	71.8	85.6	92.5	96.2

can be represented by Eq. (9). The reaction at the cathode could involve evolution of hydrogen following reduction of water Eqs. (10) and (11).

Anodic reaction:

$$M_{(s)} \rightarrow M^{2n+} + ne^- \tag{8}$$

$$Fe_{(s)} \rightarrow Fe^{2+}_{(aq)} + 2e^- \tag{9}$$

Cathodic reaction:

$$2H^+_{(aq)} + 2e^- \rightarrow H_{2(g)} \tag{10}$$

$$H_2O + e^- \rightarrow H^+ + OH^- \tag{11}$$

Potentiodynamic polarization measurement was employed to control the potential (being the driving force) in order to measure the current as a function of net change in reaction rate. A compromise current, usually known as corrosion current density (I_{corr}), and the corresponding potential (E_{corr}) was obtained from rationalization of the anodic and cathodic branches of appropriate Tafel plots (Fig. 3). The cathodic constant (β_c) and anodic constant (β_a) and some other PDP parameters were also obtained and shown in Table 3.

The obtained I_{corr} values from PDP measurements decrease as concentration of MSE and Fe-MSE Nano solution increases, the highest values obtained being the uninhibited 1 M HCl solution. This could be attributed to the formation of adsorbed thin film of the inhibitor on the steel surface. On the other hand, E_{corr} values measured in 1 M HCl solution is more negative than those measured in the inhibited solutions. This implies that E_{corr} values are displaced to more positive regions. When corrosion inhibitors display this kind of displacement, they are usually classified as anodic inhibitors [35]. Anodic inhibitors are those that have dominant influence on the partial anodic reaction which involves retardation of rate of oxidation/corrosion of the metal. In literature, the above classification as anodic or cathodic inhibitor is held if the maximum displacement of E_{corr} in inhibited solution is up to −85 mV from that of 1 M HCl [35]. In the case of MSE and Fe-MSE Nano, the maximum displacement is not up to this value. Therefore, both MSE and Fe-MSE Nano can be regarded as mixed type inhibitors with anodic predominance [36]. That is to say, they inhibit both the iron dissolution and hydrogen evolution processes but more actively inhibiting iron oxidation. The mechanism of inhibition can be activation controlled or diffusion controlled.

The data obtained from EIS experiments were used to construct Nyquist plot (Fig. 4). Imperfect depressed semicircles similar in shape but with different diameter sizes were obtained. With the shapes being similar, the mechanism of the steel corrosion is the same in all the test solutions. The diameter size increased according to the concentration of the Fe-MSE Nano tested. The observed imperfection in shapes can be ascribed to roughness or inhomogeneity of the steel surface [37]. The appearance of a single capacitive loop suggests that the corrosion mechanism is controlled by charge transfer process [37].

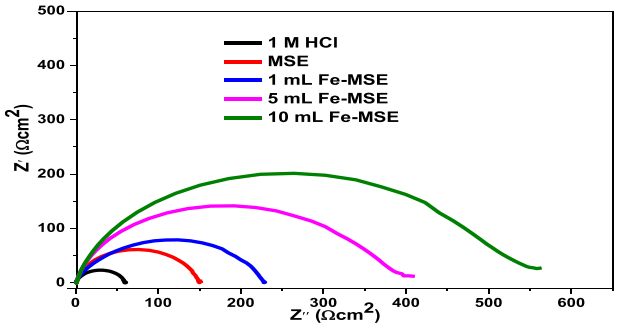

Fig. 4. Nyquist plots for mild steel corrosion inhibition in simulated descaling solution without and with MSE and different concentrations of Fe-MSE Nano.

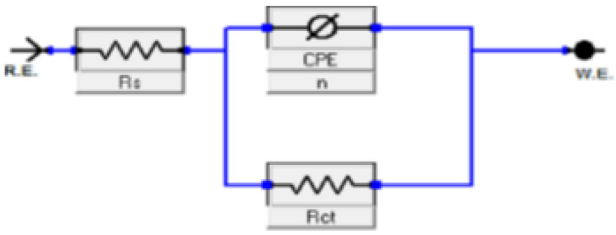

Fig. 5. Equivalent circuit used for EIS data analyses.

Table 4
EIS parameters for mild steel corrosion in 1 M HCl without and with MSE and different concentrations of Fe-MSE Nano.

EIS parameters	1 M HCl	MSE	1 mL Fe-MSE	5 mL Fe-MSE	10 mL Fe-MSE
$R_{ct}(\Omega cm^2)$	42.9	143.8	237.0	412.5	557.1
R_s (Ωcm^2)	1.124	1.215	1.238	1.312	1.318
$Y_o \times 10^{-6}$ $(\Omega^{-1} s^n cm^{-1})$	152.7	134.9	143.2	132.6	124.7
n	0.826	0.833	0.842	0.861	0.880
C_{dl} $\times 10^{-9}$ (F)	152.8	78.9	56.2	31.4	13.8
ε_{wl} (%)	–	70.2	81.9	89.6	92.3

The $R_s(R_{ct}\emptyset_{CPE})$ equivalent circuit (Fig. 5) model was used to fit the experimental data. The goodness of fit was in the order of 10^{-4}. This indicates good correlation with the model. The constant phase element (CPE) is used to compensate surface roughness or inhomogeneity of the steel [30]. The CPE can be estimated using Y_0 and n, related to impedance by Eq. (12)

$$Z_{CPE} = (Y_0)^{-1}(jw)^{-n} \tag{12}$$

where Z_{CPE} is the impedance of the CPE, Y_0 is the CPE constant, w is the angular frequency, $(j^2 = -1)$ and $n = 2\alpha/(\pi)$ given that α is the phase angle of the CPE.

Some EIS parameters calculated are presented in Table 4. The value of n is seen to increase on addition of the inhibitor, probably because the surface roughness of the steel is increased by adsorption of the inhibitor [30]. It could also be that the CPE is not a single resistance, capacitance or inductive element but a relative and/or integrated influence of all these [29]. The double layer capacitance decreases on addition of inhibitor, demonstrating increase in insulation due to adsorption of the inhibitor. The trend of inhibition efficiency obtained is also consistent with other measurements and comparable to some extents.

Scanning electron microscopy

The surface morphology of the steel surface was obtained using Scanning Electron Microscopy (SEM). Comparing the images shown in Fig. 6, it can be observed that the acid damaged the surface of the steel when the nanoparticles were not introduced. However, on introduction of the nanoparticles, the surface was protected. This further confirms that Fe-MSE Nano inhibits the steel corrosion process.

Low energy configuration and adsorption energy of Fe(1 1 1)—bananadine interaction

Adsorption Locator simulates a substrate loaded with an adsorbate [38]. This allows the lowest energy configuration of the adsorbate on the substrate to be found. By carrying out Monte Carlo searches of the configurational space of the

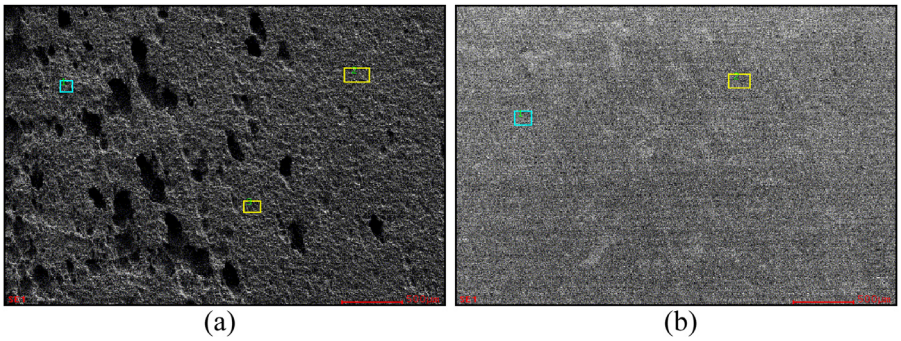

Fig. 6. SEM images of iron surface during corrosion process (a). With 1 M HCl without inhibitor (b) With 1 M HCl and inhibitor (10 mL Fe-MSE Nano).

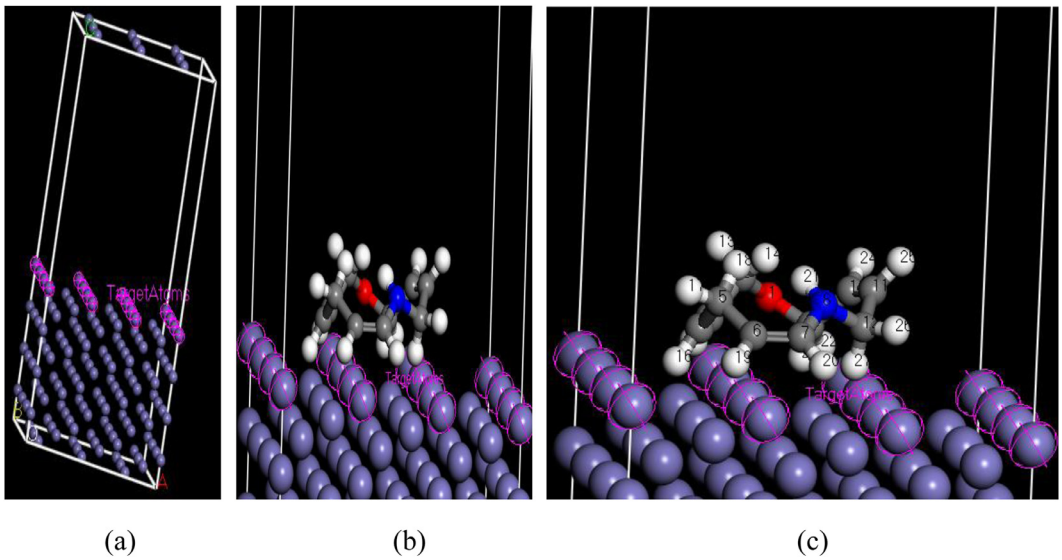

Fig. 7. Fe(1 1 1) surface-adsorbate interaction (a). Fe(1 1 1) after defining the Target Atoms set (b) low energy configuration (c) adsorbate atoms numbering.

substrate-adsorbate system, possible adsorption configurations could be identified as the temperature is slowly decreased according to a simulated annealing schedule. In order to ensure all possible configurations have been obtained, the maximum adsorbate distance and vacuum thickness were varied from 5 to 30 Å and 15–30 Å respectively. Maximum adsorbate distance of 15 Å from the selected surface target Fe atoms and a vacuum thickness of 30 Å were sufficient to record all possible configuration interactions between the bananadine molecule and Fe(1 1 1) surface avoiding interactions with periodic image or atoms from the bottom slab.

The lowest energy configuration is shown in Fig. 7(b) depicting how bananadine atoms allign on the Fe surface. The atom numbering on the adsorbate in Fig. 7(c) helps to keep track of atom allignment on the Fe surface. The bananadine molecule alligns in a similar manner, though it may be rotated horizontally along the Fe(1 1 1) surface. The preferred configuration arises due to interaction of Fe atoms with bananadine atoms. Electrophilic centers on bananadine molecule that are likely to interact with Fe atoms are predicted from Fukui analysis (Table 5). Nitrogen atom, N(8) has the maximum positive value of 0.139 indicating the center for highest electrophilic interaction. Other high electrophilic centers include, C(6) 0.133, H(20) 0.104 and H(19) 0.103 in order of decresing electrophilic influence. The interaction of these electrophilic centers with Fe atoms (assumed to be positive centers) gives rise to the preferred configuration as the atoms are all alligned on the Fe atoms. The low HOMO-LUMO gap ($\Delta E_{\text{lumo-homo}} = 3.54$ eV) on bananadine adsorbate obtained from LUMO ($E_{\text{LUMO}} = -0.995$ eV) and HOMO ($E_{\text{HOMO}} = -4.532$ eV) frontier orbitals indicates expedited adsorption process through electron density transport between Fe atoms and the electrophilic centers on bananadine molecule. The number of electrons transported ΔN can be calculated using Eq. (13):

$$\Delta N =\rightarrow X_{Fe} - -X_{ads-mol}/[2(\eta_{Fe} + \eta_{ads-mol})] \tag{13}$$

where X_F and $X_{\text{ads-mol}}$ are the electronegativity values of iron and the adsorbate molecule, respectively, η_{Fe} and $\eta_{\text{ads-mol}}$ are the global hardness of iron and the adsorbate molecule, respectively. The X_F and η_{Fe} values are 7.0 eV and 0 eV (theoretical values), respectively. The value of $X_{\text{ads-mol}}$ was obtained from the calculation $X_{\text{ads-mol}} = (\text{IE} + \text{EA})/2$, where IE is ionization

Table 5
Fukui indices for electrophilic interaction (f^-) of Fe(1 1 1) and bananadine adsorbate.

Atom	Mulliken	Atom	Mulliken
O (1)	0.030	H (14)	0.011
C (2	−0.021	H (15)	0.051
C (3)	0.029	H (16)	0.043
C (4)	−0.032	H (17)	0.069
C (5)	−0.032	H (18)	0.024
C (6)	0.133	H (19)	0.103
C (7)	0.039	H (20)	0.104
N (8)	0.139	H (21)	0.072
C (9)	−0.007	H (22)	0.046
C (10)	0.018	H (23)	−0.039
C (11)	−0.022	H (24)	0.055
C (12)	−0.048	H (25)	0.059
H (13)	0.046	H (26) 0.037	
H (27)	0.092		

Table 6
Adsorption parameters for Fe(1 1 1)-bananadine interaction using adsorption locator (adsorbate energy = −1.6526033 kcal/mol).

Lowest energy Configuration kcal/mol	Fe atomic Layer	Total energy kcal/mol	Adsorption energy kcal/mol	Rigid adsorption energy kcal/mol	Deformation energy kcal/mol
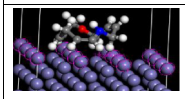	Top	-106.49846526	-104.84584493	-93.23584624	-11.60999869
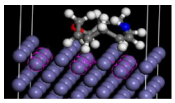	Shallow	-106.49846504	-104.84584470	-93.23572954	-11.61011516
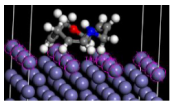	Deep	-106.49846319	-104.84584286	-93.23559088	-11.61025198
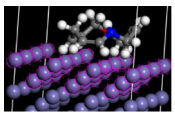	Top, shallow and deep	-106.49846109	-104.84584076	-93.23555854	-11.61028222

potential (-E_{HOMO}) and EA is electron affinity (-E_{LUMO}). Global hardness of the adsorbate molecule $\eta_{ads\text{-}mol}$ was obtained from the calculation $\eta_{ads\text{-}mol} = (IE - EA)/2$ [39]. A low number of electrons transferred ($\Delta N = 1.20 \leq 3.6$) is consistent with the fact that the major mechanism for the adsorption process is the donation of electrons from the bananadine to the iron surface [40].

Different Fe atomic layers were used for the adsorption calculation in order to understand adsorption process beyond the surface layer. The surface Fe layer is represented as Fe_{top} while the second and third Fe layers of atoms are represented as Fe_{shal} (shallow) and Fe_{deep} (deep), respectively. The three layers were also used together for the adsorption process and represented as Fe_{tsd} (top-shallow-deep). The lowest total energy obtained for Fe_{top}, Fe_{shal}, Fe_{deep} and Fe_{tsd} are presented in Table 6. The total energy of Fe_{top} atoms is more negative compared to Fe_{shal} and Fe_{deep} which implies a better adsorption process. It can therefore be inferred that a better adsorption process occurs at the top layer of Fe atoms compared to other layers.

The most important parameter from Adsorption Locator is the adsorption energy, which consists of the rigid adsorption energy and deformation energy. The rigid adsorption energy is the energy required when the unrelaxed adsorbate components are adsorbed on the substrate. In other words, the energy required for the adsorbate to attach to the surface. The rigid adsorption energy is seen to increase slightly by 11.67×10^{-5} kcal/mol between the top and shallow layers, and 13.87×10^{-5} kcal/mol between the shallow and deep layers. This means that it requires more energy for the adsorbate to get attached to other Fe layers (shallow and deep atoms). The deformation energy (energy released when the adsorbed banana-

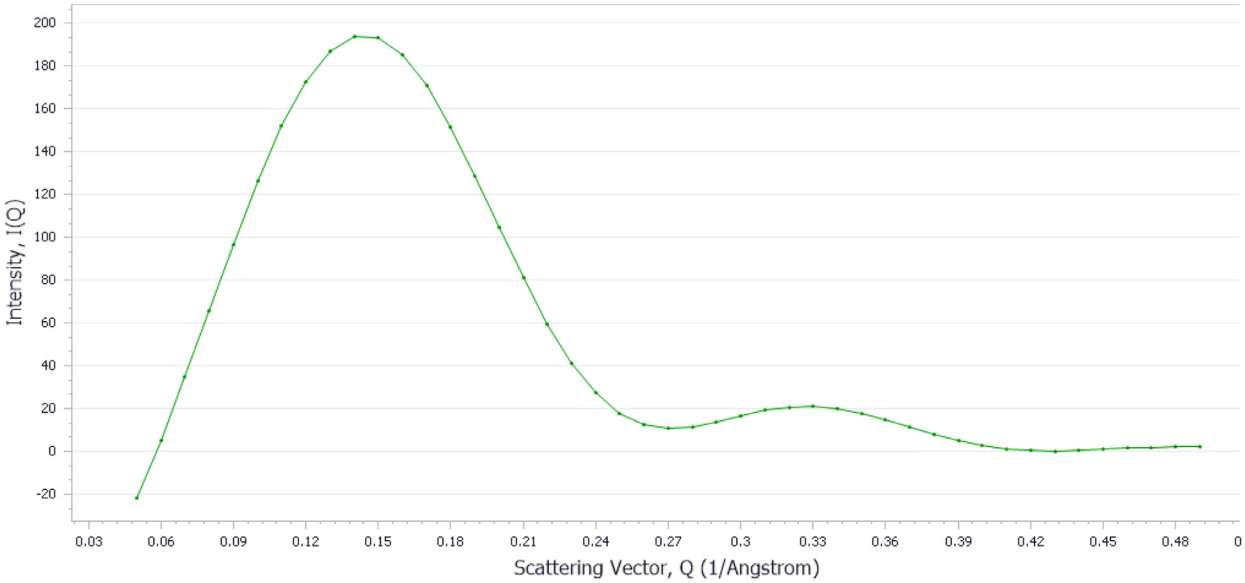

Fig. 8. Forcite neutron scattering analysis on Fe(1 1 1) atoms with bananadine adsorbate.

dine components are relaxed on the Fe surface) decreases clearly as more subatomic layers are penetrated. This implies that it requires more energy to relax the adsorbate on the top Fe atoms than shallow and deep atoms. The small difference in deformation energy between atomic layers (11.65×10^{-5} kcal/mol between top and shallow layers and 13.82×10^{-5} kcal/mol between the shallow and deep layers) indicates that bananadine can offer similar coverage to the first three atomic layers of Fe as corrosion inhibitor without much loss in energy due to infiltration of sublevels of atom [41].

An interesting fact about the adsorption and deformation energies is their direct linear relationship. As more energy is used to relax the adsorbate on the surface, the better the adsorption process on that surface. Therefore, a better relaxed adsorbate provides a better coverage which increases protection of the surface by the adsorbed molecule (inhibitor). Hence, a good inhibitor exhibits good adsorption properties. An expression which may evaluate a constant, characteristic of Fe surface was obtained as shown in Eq. (14).

$$A_{k=}E_{Def}/E_{Ads} \tag{14}$$

where $_{=}E_{Def}$ is the deformation energy and E_{Ads} is the adsorption energy. The expression yields a constant, $A_k = 0.11074$ for the Fe layers and even with all the three layers were used together for the adsorption process. This value may be unique to Fe surface and different metal, non-metal or polymer surfaces may give different values characteristic of that surface [42].

Energy of penetration of adsorbate through Fe layers

The total energy reported by Adsorption Locator integrates adsorption energy, deformation energy, rigid adsorption energy and adsorbate energy. The energy of substrates (Fe atoms) is constant throuhout the process and assumed to be 0.00 kcal/mol. The total energy can then be used to model the energy of penetration of adsorbate through the Fe atomic layers as follows:

$$E_{LPE} = \Delta E_{tot(L1/L2)} \tag{15}$$

where E_{LPE} is the layer penetration energy which represent the energy it takes for the adsorbate to infiltrate the atomic layers and $\Delta E_{tot(L1/L2)}$ is the difference in total energy between the respective atomic layers (L1 and L2). Between top and shallow layers of Fe atoms, bananadine requires an energy of 2.2×10^{-7} kcal/mol to penetrate that level, and an energy of 18.5×10^{-7} kcal/mol to breach the shallow and deep layers.Thus, it is more difficult to penetrate deeper atomic layers as indicated by this results. This is the major factor limiting good adsorption process on subatomic levels since more energies are commited to penetrating the atomic levels resulting in poor adsorption behavior.

Forcite neutron scattering analysis of adsorbate coverage on Fe(1 1 1) surface

Neutron scattering analysis was performed with and without the bananadine adsorbate loaded on Fe(1 1 1) surface. This process allows the evaluation of the extent of coverage provided by bananadine adsorbate molecule on the Fe(1 1 1) surface (Figs. 8 and 9). It is inferred from the results of neutron scattering analysis that there is suitable (resonable) coverage of bananadine molecule on Fe surface. Neutron scattering was more intense (237.56) with Fe(1 1 1) atoms alone than Fe atoms with adsorbate coverage (194.09). The bananadine could be seen to provide a protective shield on Fe surface which results

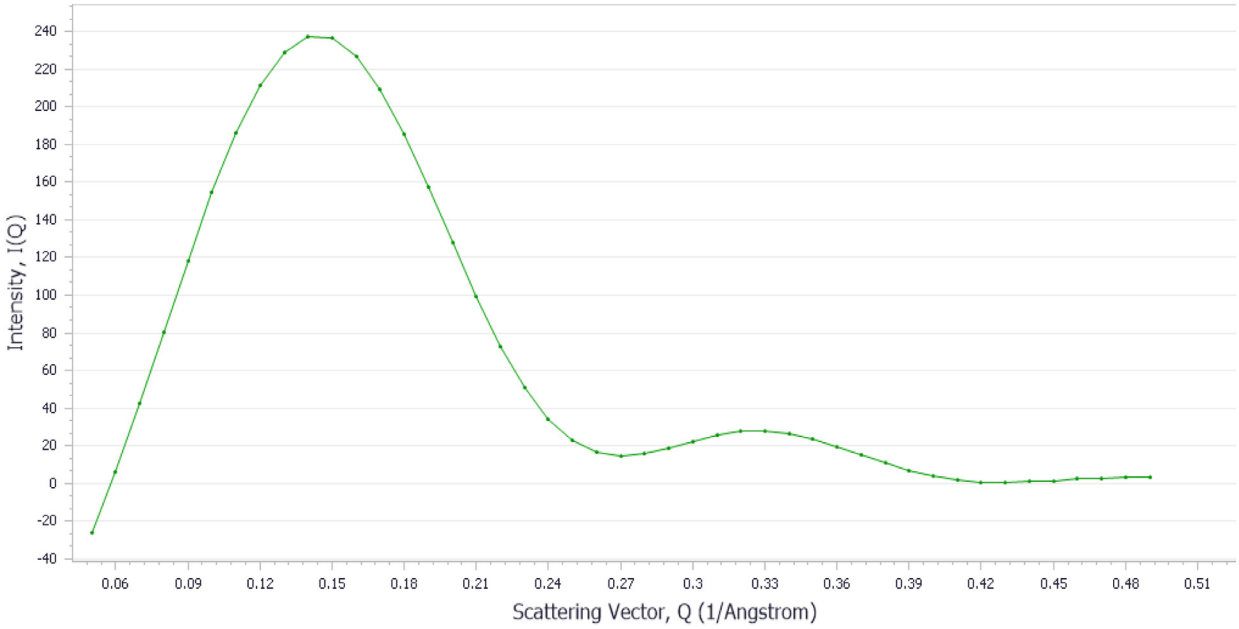

Fig. 9. Forcite neutron scattering analysis on Fe(1 1 1) atoms.

in different scattering behavior. Since neutrons are scattered by the nucleus itself and Fe nucleus is more massive compared to the atoms in bananadine, the scattering pattern from Fe nucleus is more intense. This shows that bananadine provides a suitable coverage needed for corrosion inhibition of Fe surface.

Conclusion

Iron nanoparticles mediated by Musa sapientum peels extract (Fe-MSE Nano) was investigated as anticorrosive additive in descaling liquor using thermogravmetric and electrochemical and SEM techniques. The nanoparticles were formed within 20 min of reaction of MSE with $FeCl_2$ forming a brownish colloid. Fe-MSE Nano inhibits the corrosion better than MSE at all temperatures studied. The average inhibition efficiency is 94.4% at 30 °C for 10 mL *Musa sapientum* extract-iron oxide nanoparticle composite (Fe-MSE Nano). Charge transfer resistance increases as concentration of Fe-MSE Nano per volume of descaling solution increases. Addition of Fe-SE Nano decreases double layer capacitance and corrosion current density. Fe-MSE Nano acts as mixed type inhibitor with anodic predominance. SEM image of the steel surface in the descaling liquor containing Fe-MSE Nano shows smooth surface while that of the liquor alone is highly rough depicting great attacked by the acid. Adsorption of Fe-MSE Nano was facilitated by its active compound, bananadine, through the nitrogen sites. Quantum chemical calculations indicate donation of electrons from bananadine to Fe as the major inhibition mechanism. The adsorption energy of bananadine on Fe(1 1 1) surface reveals a better inhibition at the Fe surface atoms. HOMO-LUMO energy gap ($\Delta E_{lumo\text{-}homo} = 3.54$ eV) on bananadine adsorbate frontier orbitals was low and indicates expedited adsorption process through electron density transport between Fe atoms and the electrophilic centers on bananadine moleculeFe-MSE Nano can be deployed as a better alternative anticorrosive additive for descaling solutions used in oilfield operations than the crude MSE.

Supplementary material

Supplementary material associated with this article can be found, in the online version, at doi:10.1016/j.sciaf.2019.e00075.

References

[1] A.B. Merdhah, A.A. Yassin, Scale formation in oil reservoir during water injection at high-salinity formation water, J. Appl. Sci. 1 (21) (2007) 3198–3207.
[2] Mackay, E.J. Oilfield Scale: a new integrated approach to tackle an old foe. Presented as an SPE Distinguished Lecture. 2007
[3] J. Li, M. Tang, Z. Ye, L Chen, Y. Zhou, Scale formation and control in oil and gas fields: a review, J. Disper. Sci. Technol. 38 (5) (2007) 661–670.
[4] J.R Becker, Corrosion and Scale Handbook, PennWell Books, 1998.
[5] J Fink, Petroleum Engineer's Guide to Oil Field Chemicals and Fluids, Gulf Professional Publishing, 2015.
[6] N. Ghorbani, M.C.T. Wilson, N. Kapur, N. Fleming, T. Tjomsland, A. Neville, Adsorption of polyphosphinocarboxylic acid (PPCA) scale inhibitor on carbon nanotubes (CNTs): a prospective method for enhanced oilfield scale prevention, J. Petrol. Sci. Eng. 150 (2017) 305–311.
[7] A. Kan, M. Tomson, Scale prediction for oil and gas production, SPE J. 17 (2012) 362–378.
[8] M.S. Tahir, M. Saleem, Experimental study of chemical De-scaling-I: effect of acid concentration, J. Faculty .Eng. Technol. 2007 (2008) 1–9.

[9] L. Sanders, X. Hu, E. Mavredaki, V. Eroini, R. Barker, A. Neville, Assessment of combined scale/corrosion inhibitors–A combined jar test/bubble cell, J. Petrol. Sci. Eng. 118 (2014) 126–139.
[10] F. Zucchi, I.H. Omar, Plant extracts as corrosion inhibitors of mild steel in HCl solutions, Surf. Technol. 24 (1985) 391–399.
[11] S. Mo, H.Q. Luo, N.B. Li, Plant extracts as "green" corrosion inhibitors for steel in sulphuric acid, Chem. Papers 70 (2006) 1131–1143.
[12] M.S. Al-Otaibi, A.M. Al-Mayouf, M. Khan, A.A. Mousa, S.A. Al-Mazroa, H.Z. Alkhathlan, Corrosion inhibitory action of some plant extracts on the corrosion of mild steel in acidic media, Arab. J. Chem. 7 (2014) 340–346.
[13] M. Sangeetha, S. Rajendran, J. Sathiyabama, P. Prabhakar, Eco friendly extract of Banana peel as corrosion inhibitor for carbon steel in sea water, J. Nat. Prod. Plant Resour. 2 (2012) 601–610.
[14] A. Bankar, B. Joshi, A.R. Kumar, S. Zinjarde, Banana peel extract mediated novel route for the synthesis of silver nanoparticles, Colloids Surf. A 368 (2010) 58–63.
[15] G.J. Zhou, S.H. Li, Y.C. Zhang, Y.Z. Fu, Biosynthesis of CdS nanoparticles in banana peel extract, J. Nanosci. Nanotechnol. 14 (2014) (2014) 4437–4442.
[16] H.M. Ibrahim, Green synthesis and characterization of silver nanoparticles using banana peel extract and their antimicrobial activity against representative microorganisms, J. Radiat. Res. Appl. Scie. 8 (2015) (2015) 265–275.
[17] A. Narayanamma, Natural synthesis of silver nanoparticles by banana peel extract and as an antibacterial agent, IOSR J. Polymer Textile Eng. 3 (2016) 17–25 2016.
[18] M. Khalil, B.M. Jan, C.W. Tong, M.A. Berawi, Advanced nanomaterials in oil and gas industry: design, application and challenges, Appl. Energy 191 (2017) 287–310.
[19] M.C. Li, Q. Wu, K. Song, Y. Qing, Y. Wu, Cellulose nanoparticles as modifiers for rheology and fluid loss in bentonite water-based fluids, ACS Appl. Mater. Interf. 7 (2015) 5006–5016.
[20] S. Gómez-Graña, M. Perez-Ameneiro, X. Vecino, I. Pastoriza-Santos, J. Perez-Juste, J.M. Cruz, A.B. Moldes, Biogenic synthesis of metal nanoparticles using a biosurfactant extracted from corn and their antimicrobial properties, Nanomaterials 7 (2017) 139–146.
[21] K. Jagajjanani, Aegle marmelos leaf extract and plant surfactants mediated green synthesis of Au and Ag nanoparticles by optimizing process parameters using taguchi method, ACS Sustain. Chem. 3 (2015) 483–491.
[22] A. Johnson, I. Obot, U. Ukpong, Green synthesis of silver nanoparticles using Artemisia annua and Sida acuta leaves extract and their antimicrobial, antioxidant and corrosion inhibition potentials, J. Mater. Environ. Sci. 5 (2014) 899–906.
[23] E.A. Essien, D. Kavaz, E.B. Ituen, S.A. Umoren, Synthesis, characterization and anticorrosion property of olive leaves extract-titanium nanoparticles composite, J. Adhes. Sci. Technol. 32 (2018) 1773–1794.
[24] M. Idrees, S. Batool, T. Kalsoom, S. Raina, H.M.A. Sharif, S. Yasmeen, Biosynthesis of silver nanoparticles using Sida acuta extract for antimicrobial actions and corrosion inhibition potential, Environ. Technol. 40 (8) (2018) 1071–1078.
[25] E. Ituen, O. Akaranta, A. James, Green anticorrosive oilfield chemicals from 5-hydroxytryptophan and synergistic additives for X80 steel surface protection in acidic well treatment fluids, J. Molecular Liquids 224 (2016) 408–419.
[26] S.K. Nayak, M. Nooijen, S.L. Bernasek, P. Blaha, Electronic structure study of CO adsorption on the Fe (001) surface, J. Phys. Chem. B 105 (2001) 164–172.
[27] A. Stibor, G. Kresse, A. Eichler, J. Hafner, Density functional study of the adsorption of CO on Fe (1 1 0), Surf. Sci. 507 (2002) 99–102.
[28] S.P. Mehandru, A.B. Anderson, Binding and orientations of CO on Fe (110),(100), and (111): a surface structure effect from molecular orbital theory, Surf. Sci. 201 (1998) 345–360.
[29] N.D. Spencer, R.C. Schoonmaker, G.A. Somorjai, Iron single crystals as ammonia synthesis catalysts: effect of surface structure on catalyst activity, J. Catalysis 74 (1982) (1982) 129–135.
[30] Agbaje Lateef, Musibau A. Azeez, Tesleem B. Asafa, Taofeek A. Yekeen, Akeem Akinboro, Iyabo C. Oladipo, Luqmon Azeez, Sunday A. Ojo, Evariste B. Gueguim-Kana, Lorika S. Beukes, Cocoa pod husk extract-mediated biosynthesis of silver nanoparticles: its antimicrobial, antioxidant and larvicidal activities, J. Nanostruct. Chem. 6 (2016) 159–169.
[31] E. Ituen, O. Akaranta, A. James, Evaluation of performance of corrosion inhibitors using adsorption isotherm models: an overview, Chem. Sci. Int. J.l 18 (2016) 1–34.
[32] O.S. Amodu, M.O. Odunlami, J.T. Akintola, S.K. Ntwampe, S.M. Akoro, Exploring Musa paradisiaca peel extract as a green corrosion inhibitor for mild steel using factorial design method, Corrosion Inhibitors., IntechOpen, 2019, doi:10.5772/intechopen.82617.
[33] B. Senthilvadivu, V. Aswini, K.S. Kumar, Anti-corrosive behavior of ethanolic extract of banana peel against acidic media and their thermodynamic studies, Int. J. Sci. Res. 6 (2007) 1762–1768.
[34] B. Delley, From molecules to solids with $Dmol^3$ approach, J. Chem. Phys. 113 (2000) 7756–7764.
[35] J.P. Perdew, Y. Wang, Accurate and simple representation of the electron-gas correlation energy, Phys. Rev. B 45 (1992) 13244–13249.
[36] F. Ortmann, F. Bechstedt, W.G. Schmidt, Semiempirical van der Waals correction to the density functional description of solids and molecular structures, Phys. Rev. B 73 (2006) 205101–205110.
[37] J. Jena, N. Pradhan, B.P. Dash, P.K. Panda, B.K. Mishra, Pigment mediated biogenic synthesis of silver nanoparticles using diatom Amphora sp. and its antimicrobial activity., J. Saudi Chem. Soc. 19 (2015) 661–666.
[38] K.K. Anupama, K. Ramya, K.M. Shainy, A. Joseph, Adsorption and electrochemical studies of Pimenta dioica leaf extracts as corrosion inhibitor for mild steel in hydrochloric acid, Mater. Chem. Phys. 167 (2015) 28–41.
[39] A.S. Fouda, M.A. Ismail, G.Y. EL-ewady, A.S. Abousalem, Evaluation of 4-amidinophenyl-2, 2′-bithiophene and its aza-analogue as novel corrosion inhibitors for CS in acidic media: experimental and theoretical study, J. Mol. Liq. 240 (2017) 372–388.
[40] V. Cerný, A thermodynamic approach to the travelling salesman problem: an efficient simulation algorithm, J. Optim. Theor. Appl. 45 (1985) 41–51.
[41] R.G. Parr, R.G. Pearson, Absolute hardness: companion parameter to absolute electronegativity, J. Am. Chem. Soc. (1983) 7512–7516..
[42] P. Udhayakala, Quantum chemical studies on the inhibition potentials of thiophene derivatives for the corrosion inhibitors of carbon steel, J. Chem. Pharm. Res. 7 (2015) 803–810.